



ELSEVIER

Contents lists available at [SciVerse ScienceDirect](http://www.sciencedirect.com)

Comptes Rendus Physique

www.sciencedirect.com

Crystal growth / Croissance cristalline

Growth of a strained epitaxial film on a patterned substrate

*Croissance d'un film épitaxié contraint sur un substrat patterné*Xianbin Xu^a, Jean-Noël Aqua^{a,*}, Thomas Frisch^b^a Institut des nanosciences de Paris, université Pierre-et-Marie-Curie-Paris-6, CNRS UMR 7588, 4, place Jussieu, 75252 Paris, France^b Institut non linéaire de Nice, université de Nice-Sophia Antipolis, CNRS UMR 6618, 1361, routes des Lucioles, 06560 Valbonne, France

ARTICLE INFO

Article history:

Available online 1 February 2013

*Keywords:*Strained epitaxial film
Asaro–Tiller–Grinfel'd instability
Patterning*Mots-clés:*Film épitaxié contraint
Instabilité d'Asaro–Tiller–Grinfel'd
Structuration

ABSTRACT

We study the influence of the growth kinetics on the Asaro–Tiller–Grinfel'd instability of a thin film deposited on a patterned substrate. We use a continuum model that we solve at first order in the surface slope. Both wetting interactions and elastic fields induced by the film/substrate interface introduce an explicit dependence on the film thickness. As a consequence, the translational symmetry in the growth direction is broken and the deposition flux cannot be trivially accounted for. Similarly to the evolution during annealing, the instability can skip during growth from an in-phase to an out-of-phase geometry depending on the growth duration and film thickness. We compare the evolution of the instability using different deposition fluxes. We find that the kinetic phase diagram found in the annealing case also explains the evolution during growth in usual growth conditions.

© 2012 Académie des sciences. Published by Elsevier Masson SAS. All rights reserved.

R É S U M É

Nous étudions l'influence de la cinétique de croissance sur l'instabilité d'Asaro–Tiller–Grinfel'd qui se développe sur un film mince sur un substrat structuré. Nous utilisons un modèle continu qui est résolu au premier ordre en la pente de la surface. Les interactions de mouillage ainsi que le champ élastique induit par l'interface film/substrat introduisent une dépendance explicite dans l'épaisseur du film. En conséquence, la symétrie par translation dans la direction de croissance est brisée et le flux de déposition n'est pas un paramètre trivial de l'instabilité. Comme dans le cas du recuit, nous trouvons que l'instabilité peut évoluer d'une configuration en phase vers une configuration en opposition de phase avec le substrat, en fonction du temps de déposition et de l'épaisseur du film. Nous comparons l'évolution de l'instabilité pour différents flux de croissance. Le diagramme des phases cinétique obtenu dans le cas du recuit rend aussi compte de l'évolution du film lors de la croissance dans ses conditions courantes.

© 2012 Académie des sciences. Published by Elsevier Masson SAS. All rights reserved.

* Corresponding author.

E-mail address: aqua@insp.jussieu.fr (J.-N. Aqua).

1. Introduction

Controlling the self-organization of quantum dots is a requirement for their potential use in optical or electronic systems. Their position, geometry and size distribution need to be precisely defined if one wants to draw benefit of their physical properties. This control addresses fundamental questions regarding the growth mechanisms of quantum dots (QDs) and the interplay between self-organization and an external forcing. The coherent deposition of a crystal film on a lattice-mismatched substrate is known to be a good way to generate QDs following the Stransky–Krastanov growth mode, where strain relaxation leads to an island after the completion of a wetting layer [1,2]. However, when grown on a flat substrate, the randomness of surface diffusion leads to disordered objects with a significant size dispersion. Recent developments have been made to combine the strain induced self-assembly with surface patterning in an effort to improve the size uniformity and spatial order [3].

Different kinds of templates have been dedicated to the growth of quantum dots using optical lithography, e-beam lithography, focused ion-beam (FIB), vicinal substrates, growth instabilities, etc. [3–9]. In some conditions, a strong correlation is found between the pattern and the growing islands leading to regular arrays. For example, Ge dots grown on stripes and mesas revealed ordering on the top concave part of the template [10–13]. On the contrary, pit-patterned substrates produced by holographic lithography in the sub-micrometer range lead to ordering of islands inside the pits, i.e. in the bottom convex part of the pattern, see e.g. Ref. [14], as found in similar geometries [15–18]. More recently, experiments on FIB nano-patterns [3,19] evidenced the influence of the temperature: while islands nucleate at low temperature inside the pits, they nucleate outside at high temperature and randomly at intermediate temperature.

On the theoretical front, no clear and comprehensive description of the preferential growth of islands on a pattern arises. As regards equilibrium, Yang, Liu and Lagally [13] showed that local minima of the surface chemical potential arise in convex regions due to an enhanced strain relaxation, so that growth should occur preferentially on top of the pattern. On the other hand, Monte Carlo simulations [19] showed that equilibrium corresponds to dots sitting between holes, whereas metastable states are found at low T , where dots grow in the pits. Finally, note that a simple calculation assuming a sinusoidal surface and pattern shapes [20] showed that the geometry which minimizes the energy corresponds to a substrate out-of-phase with respect to the substrate where the surface maxima lie on top of the substrate minima. As regards kinetics, the computation of the variation of the nucleation barrier due to the sole elastic relaxation showed that nucleation should be directed in the bottom of a pit [21]. Finally, kinetic Monte Carlo simulations using a basic description of elastic relaxation with a given chemical potential for different islands volume, argued that, whereas the most energetically favorable sites are in the center of the pits, nucleation occurs randomly at low T , and preferentially in the holes at intermediate and high T , the latter undergoing a significant Ostwald ripening. Our goal is to clarify the different outcomes and to investigate the ordering resulting from the diffusion equation on a surface which describes the essential mechanisms at work on large scales.

The island growth may follow different pathways. In SiGe systems, islands nucleate spontaneously during an abrupt 2D–3D transition when the strain is high enough, i.e. concerning a $\text{Si}_{1-x}\text{Ge}_x$ film on Si, when x is high enough. However, when the strain is not too large, the island growth follows an initial nucleationless morphological instability [22] reminiscent of the Asaro–Tiller–Grinfeld (ATG) instability [23,24]. The absence of nucleation in this case is a promising route for increasing the spatial order resulting from the island self-organization, especially when growth occurs on top of a patterned substrate. We aim here at describing the evolution governing this instability on a patterned substrate. We performed in Ref. [25] a linear analysis of this instability on a pattern for a given film thickness. It corresponds to experiments where one grows a film on a time scale where mass transport does not have time to occur, and then performs annealing where the instability occurs. We investigate here the influence of the growth kinetics on the instability development and study the evolution during deposition also and its dependence on the flux.

We consider a continuum model describing surface diffusion ruled by surface energy, elastic relaxation and wetting interaction between the film and the substrate. Using a quasi-static approximation, we find the mechanical equilibrium solution within the small-slope approximation and solve the film evolution at linear order in the surface corrugation. We find different geometries depending on the pattern wavelength, film thickness, annealing time, and deposition flux. The film can either mainly develop a corrugation equal to the substrate shape but either in-phase or out-of-phase, or develop a ‘classic’ ATG-like morphology with little impact of the pattern. We compare these results with the dynamics resulting from the annealing case and find that the kinetic phase diagram which gives the typical geometry as a function of time and film thickness, is still relevant under deposition when typical growth conditions are used. Of special interest is the time where a phase shift occurs, i.e. where the instability is first in-phase with the substrate, vanishes and subsequently develops an out-of-phase configuration [25]. This change of geometry is important for the localization of the subsequent quantum dots which will grow on the basis of the instability initial stage.

2. Continuum model

We describe the hetero-epitaxial system by a film with a free surface $z = h(\mathbf{r}, t)$, where z is the growth direction and $\mathbf{r} = (x, y)$, deposited on a substrate with an interface $z = h_i(\mathbf{r})$. The lattice mismatch between the film and substrate is $m = 1 - a_f/a_s$, with the film a_f and substrate a_s lattice parameters. Mechanical equilibrium is reached on the instability time scale so that the Navier–Lamé equations, $\partial_i \sigma_{ij} = \mathbf{0}$, apply in the entire system. The film surface is supposed to be

free of stress, while the film/substrate interface is coherent, with the continuity of displacements and forces. An analytical solution of the Navier–Lamé equations can be found in Fourier space $\mathcal{F}[h](\mathbf{k}) = (2\pi)^{-2} \int d\mathbf{r} e^{i\mathbf{k}\cdot\mathbf{r}} h(\mathbf{r})$ when using the small-slope approximation for solving the interface and free film boundary conditions. Given the elastic displacements and strain tensor \mathbf{e} , one can compute the elastic energy density $\mathcal{E}^{el} = \frac{1}{2} \sigma_{ij} e_{ij}$ at first order, which reads on the surface [25]

$$\mathcal{E}^{el}(\mathbf{r}) = \mathcal{E}_0 \{1 - 2(1 + \nu)\mathcal{H}[h] + 2(1 + \nu)\mathcal{H}_i[h_i, \bar{h}]\} \quad (1)$$

where $\mathcal{E}_0 = Ym^2/(1 - \nu)$ is the elastic energy density of a flat film on a flat substrate, while ν and Y are the film Poisson ratio and Young modulus respectively. The operators

$$\mathcal{H}[h] = \mathcal{F}^{-1}[|\mathbf{k}|\mathcal{F}[h]] \quad (2)$$

$$\mathcal{H}_i[h_i, \bar{h}] = \mathcal{F}^{-1}[|\mathbf{k}|e^{-|\mathbf{k}|\bar{h}}\mathcal{F}[h_i]] \quad (3)$$

are associated respectively with the elastic dipoles induced by the free surface and to the buried dipoles of the film/substrate interface which involve the mean film thickness \bar{h} .

The morphological evolution that we study is ruled solely by surface diffusion, which is relevant for experiments at not too high temperature where intermixing could also come into play. The diffusion flux on the surface enforces the mass conservation equation

$$\frac{\partial h(\mathbf{r}, t)}{\partial t} = D\Delta_s \mu + F \quad (4)$$

where D is a surface diffusion coefficient, Δ_s is the surface Laplacian, μ is the chemical potential and F is the deposition flux. The chemical potential μ is the sum of the elastic energy on the surface $\mathcal{E}^{el}(\mathbf{r})a_f^3$, and a term describing the surface energy. Wetting interactions between the film and the substrate induce a dependence of the surface energy on the film thickness h when the latter is a few atomic layer large. In order to depict SiGe systems where a small variation of γ is found [26], we decompose the latter dependence as $\gamma(h) = \gamma_f(1 + \delta\gamma_h)$, where γ_f is the pure film surface energy while $\delta\gamma_h = c_w \exp(-h/\delta_w)$, with the amplitude c_w and decay length δ_w . Given that the local thickness is $h(\mathbf{r}) - h_i(\mathbf{r})$, we consider on a patterned substrate the dependence $\gamma(h - h_i)$. The surface contribution to the chemical potential is thence $\gamma(h - h_i)\kappa + \frac{\partial\gamma}{\partial h} \frac{1}{\sqrt{1+|\nabla h|^2}}$, where κ is the surface curvature equal to $-\Delta h$ at first order in the surface slope. Eventually, in units of the space and time scales $l_0 = \gamma_f/2(1 + \nu)\mathcal{E}_0$ and $t_0 = l_0^4/D\gamma_f$, the evolution equation at first order in the surface and interface slopes reads

$$\frac{\partial h}{\partial t} = \Delta \{-\Delta h - \mathcal{H}[h] + \mathcal{H}_i[h_i] + a(\bar{h})(h - h_i)\} + F \quad (5)$$

with the amplitude of the wetting term $a(\bar{h}) = c_w e^{-\bar{h}/\delta_w}/\delta_w^2$.

For a given film thickness \bar{h} on a flat substrate, a single mode modulation of the film surface $e^{i\mathbf{k}\cdot\mathbf{r}}$ grows as $e^{\sigma t}$ with the growth rate

$$\sigma(\mathbf{k}; \bar{h}) = -a(\bar{h})\mathbf{k}^2 + |\mathbf{k}|^3 - \mathbf{k}^4 \quad (6)$$

The typical $|\mathbf{k}|^3 - \mathbf{k}^4$ spectrum corresponds to the usual ATG instability which is hindered by the $-\mathbf{k}^2$ wetting term, as wetting favors the surface to follow the pattern shape. Below a given thickness h_c , σ is negative for every \mathbf{k} and the instability is suppressed due to wetting interactions [27], as usual in the Stransky–Krastranov growth mode. On the contrary, above h_c , the instability grows and we define for convenience $k_{\text{ATG}} = 3/4$ as the wave-vector which maximizes the ATG growth rate when no wetting interactions are at work, and which defines the typical length scale of the ATG instability. The influence of the forcing terms in Eq. (5) on the morphological evolution at constant thickness \bar{h} was analyzed in Ref. [25] where we described the kinetic phase diagram of the instability: Depending on the substrate wavelength, film thickness and annealing time, the surface geometry was found either to follow exactly the pattern, to follow the pattern shape but with an anti-coincidence geometry, or to merely develop the instability typical geometry quite independently of the pattern.

In order to depict growing films and the influence of the growth kinetics, we now consider a two-step growth mode, where the film is first grown at constant deposition flux before annealing occurs, see Fig. 5. The film evolution is now explicitly function of the film thickness (\bar{h}) which depends on time. During the first step $\bar{h}(t) = h_c + Ft$, while it is constant during annealing. We do not consider the dynamics below the critical height where no evolution occurs because of strong enough wetting interactions. Once a given thickness is reached, that we choose in most cases equal to 20 monolayers (ML) for practical reasons, annealing is performed at constant thickness $\bar{h}(t) = \text{cst}$. The evolution equation at linear order (5) can be solved analytically, and one finds

$$h(\mathbf{k}, t) = h_0(\mathbf{k})e^{\sigma_k^*(t)t} + \delta(\mathbf{k})Ft + h_i(\mathbf{k})e^{\sigma_k^*(t)t} \times \dots \times \int_0^t dt' [|\mathbf{k}|^2 \delta\gamma_h''[\bar{h}(t')] - |\mathbf{k}|^3 e^{-|\mathbf{k}|\bar{h}(t')}] e^{-\sigma_k^*(t')t'} \quad (7)$$

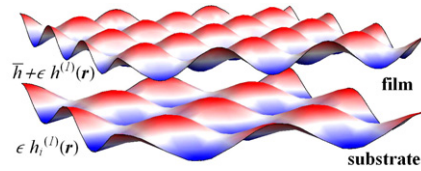


Fig. 1. (Color online.) Geometry of a film deposited on a patterned substrate with an egg-carton shape.

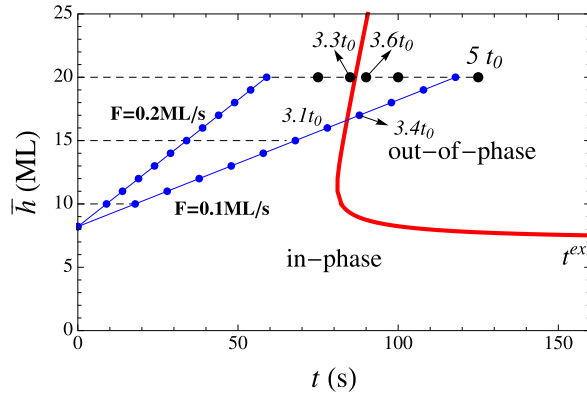


Fig. 2. (Color online.) Kinetic phase diagram for $k_i = k_{ATG}$. The red line t^{ex} characterizes the time when the instability skips from a configuration parallel to the pattern but in-phase with it to a configuration out-of-phase. The blue lines with dots show the film thickness evolution under consideration related to deposition fluxes $F = 0.1$ ML/s and $F = 0.2$ ML/s respectively. The blue points refer to the times corresponding to the deposition of each monolayer from h_c up to 20 ML, and characterize the line scans shown in Figs. 3 and 4. The black points on the horizontal line refer to the different times during annealing also shown in Figs. 3 and 4.

where $h_0(\mathbf{k})$ is the initial condition $h(\mathbf{r}, t = 0)$ in Fourier space, while we defined the time-average growth rate $\sigma_k^*(t) = \frac{1}{t} \int_0^t dt' \sigma[\mathbf{k}; \bar{h}(t')]$ and defined $\delta\gamma_h''$ as the second derivative of $\gamma(h)$ with respect to h . Eq. (7) shows that the film evolution is dictated firstly by a term linked to the initial condition h_0 which enforces a classic ATG instability dynamics. On the other hand, the term linked to h_i favors the film surface to follow the pattern geometry, in-phase if its amplitude is positive, or out-of-phase otherwise.

3. Results and discussion

In the following, we consider a substrate which displays a typical egg-carton shape, see Fig. 1, with a wave-vector modulus k_i ,

$$h_i(\mathbf{r}) = \epsilon [\cos(k_i x) + \cos(k_i y)] \quad (8)$$

where ϵ is a small parameter which ensures the small-slope approximation. When $\bar{h} < h_c$, the instability does not occur and wetting interactions enforce a surface which follows the pattern geometry. We compute the evolution after the thickness h_c and choose for the initial condition

$$h_0(\mathbf{r}) = h_c + h_i(\mathbf{r}) + \mathcal{R} \quad (9)$$

where \mathcal{R} is a white noise which describes the intrinsic deposition noise and substrate roughness that we choose to correspond to a roughness of 1 ML [25]. We perform a numerical computation of Eq. (7) using a decomposition on the Fourier modes, with the parameters appropriate for a $\text{Si}_{0.75}\text{Ge}_{0.25}$ film on a Si substrate, $c_w = 0.09$, $\delta_w = 1$ ML while $l_0 = 27$ nm [28]. At the working temperature $T = 700^\circ\text{C}$, the instability time scale is $t_0 = 25$ s. These parameters and initial condition (9) correspond to the system under study in Ref. [25]. It was shown in this reference that there exists a typical time $t^{ex}(k_i; \bar{h})$ for which the surface morphology skips during annealing from two geometries parallel to the pattern but either in- or out-of-phase, through a nearly flat configuration in between (even when the growth rate of the k_i mode is positive).

We first consider the simplest case $k_i = k_{ATG}$ where a single characteristic wavelength occurs and where the pattern influence is maximal. We plot in Fig. 2, the film thickness evolution for two different fluxes together with the t^{ex} line which results from the annealing analysis. We choose a film thickness of 20 ML while $F = 0.2$ ML/s for which growth occurs mainly in the in-phase region of the annealing phase diagram, and $F = 0.1$ ML/s, for which growth is still acting at t^{ex} . Line scans of the corresponding surface geometries at different times are plotted in Figs. 3 and 4. For the time under investigation, the surface geometry is mainly dictated by the pattern shape. It skips from an in-phase configuration to an out-of-phase one roughly at the same time t^{ex} compared to the annealing case. For this case, self-organization is found to

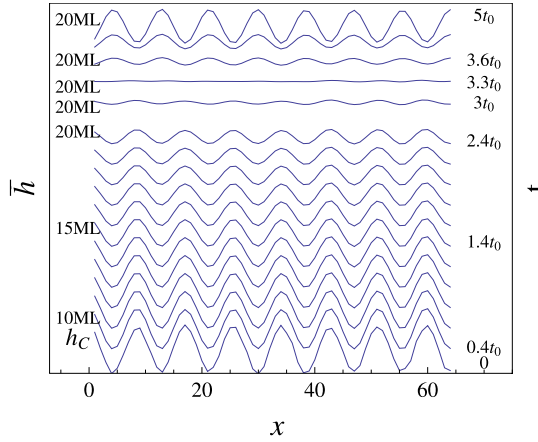


Fig. 3. (Color online.) Line scan of the surface geometry at each monolayer from initial thickness up to 20 ML during deposition and subsequent annealing, with $k_i = k_{ATG}$ and $F = 0.2$ ML/s.

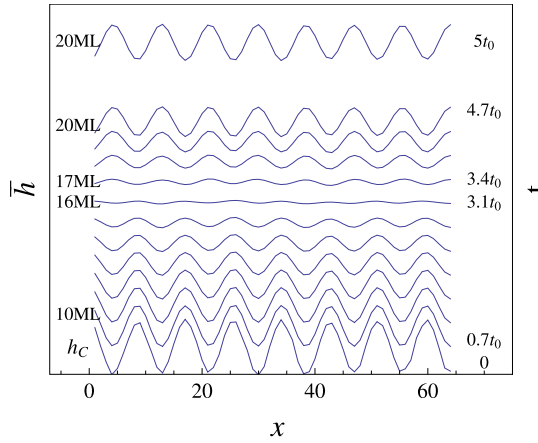


Fig. 4. (Color online.) Same characteristics as in Fig. 3 but with $F = 0.1$ ML/s. Note the change from in-phase to out-of-phase as indicated by arrows.

be perfectly controlled by the influence of the pattern with either a localization on top (initially) or in the bottom (at large time) of the pattern depending mainly on the growth duration (either growth or annealing).

We now consider the case $k_i = \frac{1}{2}k_{ATG}$, where the system is ruled by two different characteristic length scales. In this case, the dynamics results from the competition between the growth of the k_i mode, which favors a change from an in-phase to an out-of-phase configuration, and the growth of the k_{ATG} mode, which favors a typical ATG instability morphology. This instability is characterized by a moderate spatial order in real space and a ring of maxima in Fourier space. In the annealing case, beside the t^{ex} line, an extra t^{max} line characterizes the full development of the instability at k_{ATG} , see the upper black line in Fig. 5. The time t^{max} is defined in Fourier space by the fact that the spectrum $|h(\mathbf{k})|^2$ at k_{ATG} is larger than the spectrum at k_i [25]. Two growth scenarios are investigated at two different fluxes, $F = 0.1$ and 0.01 ML/s, see Fig. 5. The former corresponds nearly to the annealing case where deposition occurs quickly before any evolution occurs, while in the latter case, the surface evolution occurs already during deposition. For $F = 0.1$ ML/s, the t^{ex} line is still relevant to characterize the first vanishing of the amplitude of the k_i mode prior to its phase shift, but the surface geometry for this time gets clearly an extra noisy modulation due to the growth of the ‘classic’ k_{ATG} mode. Similarly, for $F = 0.01$ ML/s, the vanishing of the amplitude of the k_i mode is still well described by the t^{ex} line, but the subsequent growth is also clearly modified by the k_{ATG} mode. We plot in Fig. 8(a) the full geometry of the film after the shift from the in-phase to the out-of-phase geometry. The film clearly gets some noise corresponding to the k_{ATG} mode but the geometry enforced by the pattern is still clearly visible. In addition, when the deposition time exceeds the time t^{max} , the ‘classic’ instability is again fully developed, see Figs. 5 and 8(b), and overcomes the pattern mode, as seen in Fourier space in Fig. 9.

These findings put emphasis on the importance to consider a dynamical approach to investigate such structures. Minimization of energy would lead, when no wetting interactions are at work, to a geometry where the film is out-of-phase relatively to the substrate [20]. When wetting interactions are included, an in-phase configuration would be stable for thin enough films, while the out-of-phase one is again stable above a given thickness [25]. Here, we find that either states can be found depending on the time used to grow the film, with a transition from the in-phase to the elastic energy minimizing

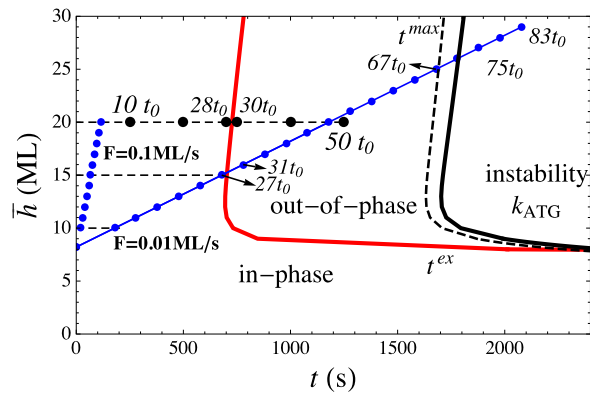


Fig. 5. (Color online.) Same notation as in Fig. 2 but for $k_i = \frac{1}{2}k_{\text{ATG}}$, and with deposition fluxes $F = 0.1$ and 0.01 ML/s corresponding respectively to the line scans in Figs. 6 and 7. The extra upper black line, referred to as the t^{max} line in the text, delimitates the region where the instability mode k_{ATG} is stronger than the k_i one. The dash line corresponds to the t^{max} line on a stripe pattern, see Fig. 10, as discussed in Appendix A.

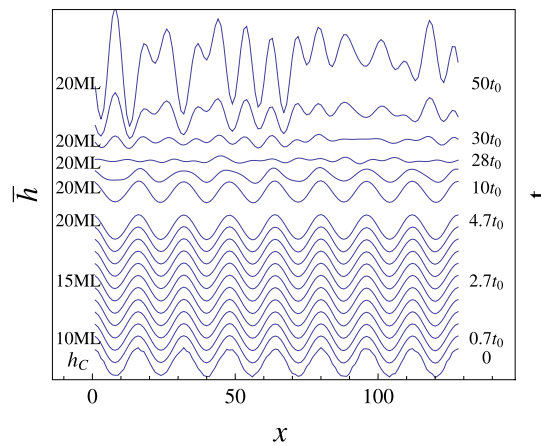


Fig. 6. (Color online.) Line scan of the surface geometry at each monolayer from initial thickness up to 20 ML during deposition and subsequent annealing, with $k_i = \frac{1}{2}k_{\text{ATG}}$ and $F = 0.1$ ML/s.

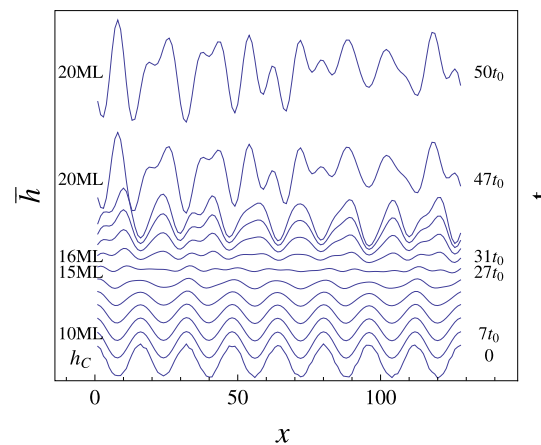


Fig. 7. (Color online.) Same characteristics as in Fig. 6 but with $F = 0.01$ ML/s.

out-of-phase geometry. Moreover, an instability with a spectrum similar to the flat substrate may be observed for a large enough deposition time. The geometry resulting from the instability defines the first stage on which quantum dots subsequently grow. Even though a systematic and explanatory comparison cannot be drawn between a simple linear analysis and

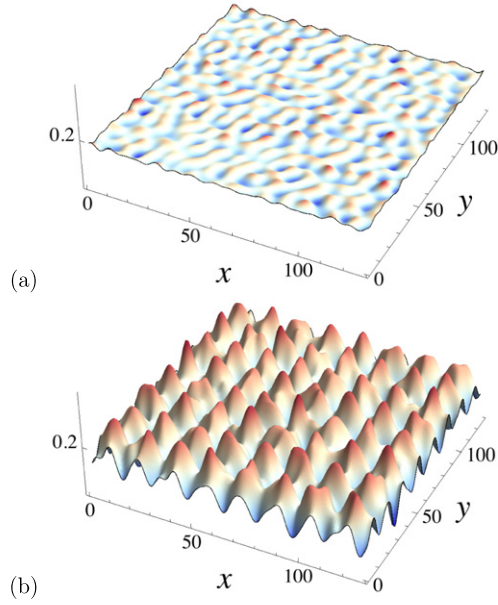


Fig. 8. (Color online.) Surface geometry with $k_i = \frac{1}{2}k_{ATG}$ and $F = 0.01$ ML/s corresponding to: (a) the time when the pattern wave-vector mode vanishes (even when it has a positive growth rate) in order to allow a shift from an in-phase to an out-of-phase configuration with respect to the pattern (corresponding to a 15 ML thick film); (b) a time after the phase shift where the instability corrugation is superimposed on an out-of-phase configuration (corresponding to a 20 ML thick film).

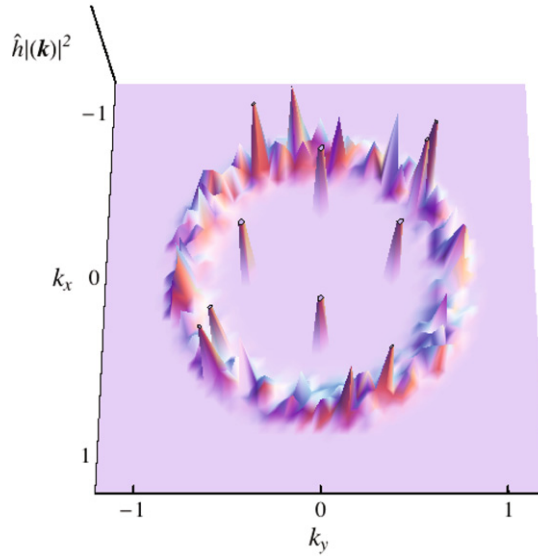


Fig. 9. (Color online.) Spectrum of the surface morphology for 25 ML deposited layers ($t = 67t_0$) for $k_i = \frac{1}{2}k_{ATG}$ and $F = 0.01$ ML/s, see the kinetic phase diagram of Fig. 5. The ring corresponds to the ‘classical’ spectrum of the ATG instability while the four peaks correspond to the pattern modes.

experiments, we believe that the kinetic phase diagram that we have exhibited gives some hints on the parameters relevant during growth and defines the basis of future work on the full non-linear regime.

4. Conclusion

We study here the dynamics of the morphological instability of a strained film on a patterned substrate. We solve the evolution equation during growth resulting from the continuum description of surface diffusion induced by elastic relaxation, surface energy and wetting interactions. We investigate the influence of the deposition flux on the initial stages of the instability in the linear approximation, and compare our findings with the results of the instability during annealing. For a given flux, we find different states (a configuration equal to the substrate geometry but either in-phase or out-of-phase, a ‘classical’ ATG instability-like morphology, etc.) depending on the time, pattern wavelength and film thickness. We study

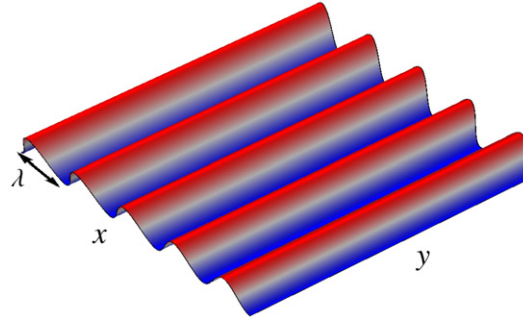


Fig. 10. (Color online.) Geometry of a 1D stripe pattern.

different growth scenarios where we deposit a given thickness but with different deposition flux and total duration of growth and annealing. We find that the kinetic phase diagram found analytically in the annealing case describes well the film configuration for a flux appropriate to describe usual growth conditions. In addition, as described in Appendix A, we also find that this kinetic phase diagram also applies to describe the film geometry in the case of a 1D stripe pattern, and is therefore likely to be relevant in many different geometries and growth scenarios. Further investigation of the fully developed island regime will require a non-linear analysis. It was already pointed out that the translational symmetry-breaking in the growth direction due to wetting interactions, enforces a non-trivial dependence on the deposition flux which leads, on a flat substrate, to different non-linear regimes [29]. Extension of the latter analysis to the patterned case, where an extra symmetry-breaking arises from the elastic interactions, is currently under investigation.

Appendix A. 1D stripe pattern

We investigate here the influence of the pattern geometry by looking at a 1D pattern, see Fig. 10, where the film/substrate interface is basically

$$h_i(\mathbf{r}) = \epsilon \cos(k_i x) \quad (10)$$

This geometry mimics stripe patterns which are also often studied in experiments. The evolution equation during annealing at linear order is merely

$$h(\mathbf{k}, t) = h^0(\mathbf{k})e^{\sigma t} - C(k, \bar{h})h_i(\mathbf{k})(e^{\sigma t} - 1) \quad (11)$$

with the surface initial condition $h^0(\mathbf{k})$ and the coefficient of the inhomogeneous solution $C(k, \bar{h})$ given in Ref. [25]. The kinetic phase diagram for both the egg-carton and stripe shapes during annealing are plotted in Figs. 2 and 5. The time for the phase exchange $t^{\text{ex}}(k_i, \bar{h})$ is the same for both patterns as it is defined in both cases by $t^{\text{ex}}(k_i, \bar{h}) = \ln[C/(C - 1)]/\sigma$. However, the t^{max} line, which delimitates when the ‘classic’ instability overcomes the pattern influence, differs slightly for these two pattern shapes, see Fig. 5. The t^{max} line is indeed slightly shifted for smaller times for the stripe pattern, as the amplitude of the k_i mode is indeed smaller in this case compared to the egg-carton shape.

References

- [1] B. Voigtänder, Fundamental processes in Si/Si and Ge/Si epitaxy studied by scanning tunneling microscopy during growth, Surf. Sci. Rep. 43 (2001) 127.
- [2] J. Stangl, V. Holý, G. Bauer, Structural properties of self-organized semiconductor nanostructures, Rev. Mod. Phys. 76 (2004) 725.
- [3] I. Berbezier, A. Ronda, SiGe nanostructures, Surf. Sci. Rep. 64 (2009) 47.
- [4] D.S.L. Mui, D. Leonard, L.A. Coldren, P.M. Petroff, Surface migration induced self-aligned InAs islands grown by molecular beam epitaxy, Appl. Phys. Lett. 66 (1995) 1620.
- [5] W. Seifert, N. Carlsson, A. Petersson, L.E. Wernersson, L. Samuelson, Alignment of InP Stranski–Krastanow dots by growth on patterned GaAs/GalnP surfaces, Appl. Phys. Lett. 68 (1996) 1684.
- [6] T. Ishikawa, S. Kohmoto, K. Asakawa, Site control of self-organized InAs dots on GaAs substrates by in situ electron-beam lithography and molecular-beam epitaxy, Appl. Phys. Lett. 73 (1998) 1712.
- [7] A. Konkar, A. Madhukar, P. Chen, Stress-engineered spatially selective self-assembly of strained InAs quantum dots on nonplanar patterned GaAs(001) substrates, Appl. Phys. Lett. 72 (1998) 220.
- [8] E.S. Kim, N. Usami, Y. Shiraki, Selective epitaxial growth of dot structures on patterned Si substrates by gas source molecular beam epitaxy, Semicond. Sci. Technol. 14 (1999) 257.
- [9] P.D. Szkutnik, A. Sgarlata, A. Balzarotti, N. Motta, A. Ronda, I. Berbezier, Early stage of Ge growth on Si(001) vicinal surfaces with an 8° miscut along [110], Phys. Rev. B 75 (2007) 033305.
- [10] T.I. Kamins, R.S. Williams, Lithographic positioning of self-assembled Ge islands on Si(001), Appl. Phys. Lett. 71 (1997) 1201.
- [11] G. Jin, J.L. Liu, S.G. Thomas, Y.H. Luo, K.L. Wang, B.-Y. Nguyen, Controlled arrangement of self-organized Ge islands on patterned Si(001) substrates, Appl. Phys. Lett. 75 (1999) 2752.
- [12] T. Kitajima, B. Liu, S.R. Leone, Two-dimensional periodic alignment of self-assembled Ge islands on patterned Si(001) surfaces, Appl. Phys. Lett. 80 (2002) 497.

- [13] B. Yang, F. Liu, M.G. Lagally, Local strain-mediated chemical potential control of quantum dot self-organization in heteroepitaxy, *Phys. Rev. Lett.* 92 (2004) 025502.
- [14] Z. Zhong, W. Schwinger, F. Schäffler, G. Bauer, G. Vastola, F. Montalenti, L. Miglio, Delayed plastic relaxation on patterned Si substrates: Coherent SiGe pyramids with dominant {111} facets, *Phys. Rev. Lett.* 98 (2007) 176102.
- [15] L. Vescan, T. Stoica, B. Hollander, A. Nassiopoulou, A. Olzierski, I. Raptis, E. Sutter, Self-assembling of Ge on finite Si(001) areas comparable with the island size, *Appl. Phys. Lett.* 82 (2003) 3517.
- [16] Z. Zhong, A. Halilovic, M. Muhlberger, F. Schaffler, G. Bauer, Ge island formation on stripe-patterned Si(001) substrates, *Appl. Phys. Lett.* 82 (2003) 445.
- [17] Z. Zhong, A. Halilovic, T. Fromherz, F. Schaffler, G. Bauer, Two-dimensional periodic positioning of self-assembled Ge islands on prepatterned Si(001) substrates, *Appl. Phys. Lett.* 82 (2003) 4779.
- [18] B. Sanduijav, D. Matei, G. Chen, G. Springholz, Shape transitions and island nucleation for Si/Ge molecular beam epitaxy on stripe-patterned Si(001) substrate, *Phys. Rev. B* 80 (2009) 125329.
- [19] A. Pascale, I. Berbezier, A. Ronda, P.C. Kelires, Self-assembly and ordering mechanisms of Ge islands on prepatterned Si(001), *Phys. Rev. B* 77 (2008) 075311.
- [20] H. Wang, Y. Zhang, F. Liu, Enhanced growth instability of strained film on wavy substrate, *J. Appl. Phys.* 104 (2008) 054301.
- [21] H. Hu, H.J. Gao, F. Liu, Theory of directed nucleation of strained islands on patterned substrates, *Phys. Rev. Lett.* 101 (2008) 216102.
- [22] P. Sutter, M.G. Lagally, Nucleationless three-dimensional island formation in low-misfit heteroepitaxy, *Phys. Rev. Lett.* 84 (2000) 4637.
- [23] R.J. Asaro, W.A. Tiller, Interface morphology development during stress-corrosion cracking: Part 1. Via surface diffusion, *Metall. Trans.* 3 (1972) 1789.
- [24] M.A. Grinfeld, Instability of the separation boundary between a nonhydrostatically stressed elastic body and a melt, *Sov. Phys. Dokl.* 31 (1986) 831.
- [25] X. Xu, J. Aqua, T. Frisch, Growth kinetics in a strained crystal film on a wavy patterned substrate, *J. Phys.: Condens. Matter* 24 (2012) 045002.
- [26] G.-H. Lu, F. Liu, Towards quantitative understanding of formation and stability of Ge hut islands on Si(001), *Phys. Rev. Lett.* 94 (2005) 176103.
- [27] J.-N. Aqua, T. Frisch, A. Verga, Nonlinear evolution of a morphological instability in a strained epitaxial film, *Phys. Rev. B* 76 (2007) 165319.
- [28] J.-N. Aqua, T. Frisch, Influence of surface energy anisotropy on the dynamics of quantum dot growth, *Phys. Rev. B* 82 (2010) 085322.
- [29] J.-N. Aqua, T. Frisch, A. Verga, Ordering of strained islands during surface growth, *Phys. Rev. E* 81 (2010) 021605.